Received 19 May 2021; accepted 22 June 2021. Date of publication 29 November 2021; date of current version 5 January 2022.

Digital Object Identifier 10.1109/OJAP.2021.3131239

A Study on the Radiation Characteristics of Microelectronic Probes

ZIYANG ZHENG [1] (Student Member, IEEE), AND YUE PING ZHANG [2] (Fellow, IEEE)

[1]Key Laboratory of Ministry of Education of Design and Electromagnetic Compatibility of High-Speed Electronic Systems, Shanghai Jiao Tong University, Shanghai 200240, China

[2]School of Electrical and Electronic Engineering, Nanyang Technological University, Singapore

CORRESPONDING AUTHOR: Y. P. ZHANG (e-mail: eypzhang@ntu.edu.sg)

ABSTRACT Microelectronic probes with the ground-signal-ground (GSG) tips have been widely used in testing integrated circuits and antennas. Yet, the radiation from probes has been rarely studied, which has been found to degrade the testing accuracy of the radiation from an antenna. In this paper, a typical ACP40-GSG-100 probe is studied from both simulation and measurement. It is confirmed that the probe radiation is caused by current on its tips, the metal probe shell strongly affects the radiated power distribution, and the ignorance of probe radiation causes error to the realized gain calculation. It is found that the probe shows a symmetrical radiation pattern for its symmetrical current distribution on the tips, the matched probe has larger realized gain than the open-ended one for about 4.8 dB because of stronger current, and the different contact positions on an impedance standard substrate (ISS) make the radiation distribution be different but hardly affect the realized gain. The strongest radiation of the probe basically locates within a narrow region near the symmetry plane of the probe, which makes it easier and faster to find the peak gain. A simple mathematical model is given to explain why low-gain probes are preferred in antenna radiation tests.

INDEX TERMS Microelectronic probes, radiation characteristics, millimeter wave, antenna measurements.

I. INTRODUCTION

DRIVEN by the development of 5G mobile communications, automotive radars, AR/VR gadgets, etc, there has been a great leap of interest in antennas operating at both FR1 and FR2 (mmWave) in recent years [1]–[7]. Such an antenna (or array) is usually integrated with a die (or dies) in a chip package and is widely known as an Antenna-in-Package (AiP) [8], [9].

Microelectronic probes were primarily designed to test integrated circuits on wafer or on die for their impedances and *S* parameters. Accurate impedance measurements with probes have become routine, owing to the availability of sophisticated probe impedance de-embedding techniques [10]–[13]. A microelectronic probe has also been an essential tool to characterize a mmWave AiP. In other words, the AiP has extended the use of probes from circuit to antenna measurements [14]–[30].

Using a probe to feed an antenna-under-test (AUT) has created a major problem, that is, the radiation from the probe itself, which interferes with the radiation from the AUT, making the accurate radiation measurement of the AUT quite challenging. The reflections/scattering/diffraction from the probe shell make the radiation pattern of the probe be quite irregular. Nevertheless, there have been some attempts to improve the radiation measurement accuracy. For example, a modal filtering method illustrated in [14] successfully separates the reflected signal and the original signal through post-processing.

In our research, we have found that an error occurs when calculating the AUT's gain due to the ignorance on the probe radiation in the common calculation process. Hence, it becomes necessary to know how the probe radiates and to find some possible ways to reduce its radiation effect. A literature survey reveals that relevant papers are few. This paper aims to fill the void by studying the radiation characteristics of a typical microelectronic probe through simulation and measurement.

This paper is organized as follows. In Section II, the antenna measurement setup, and the method to test antenna radiation are described briefly. In Section III,

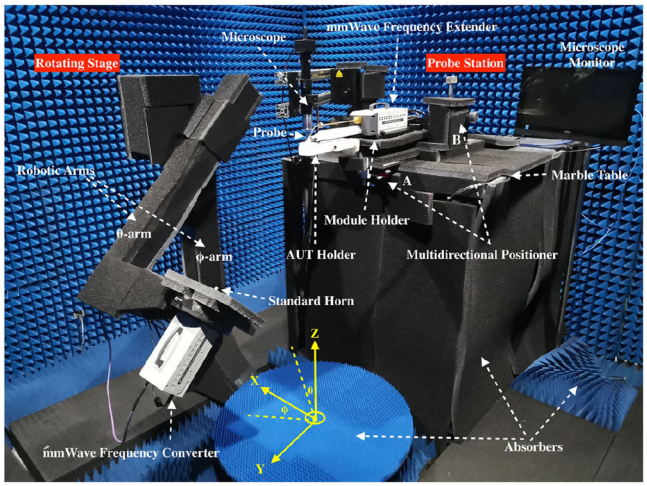

FIGURE 1. Photograph of the mmWave antenna measurement setup inside the anechoic chamber.

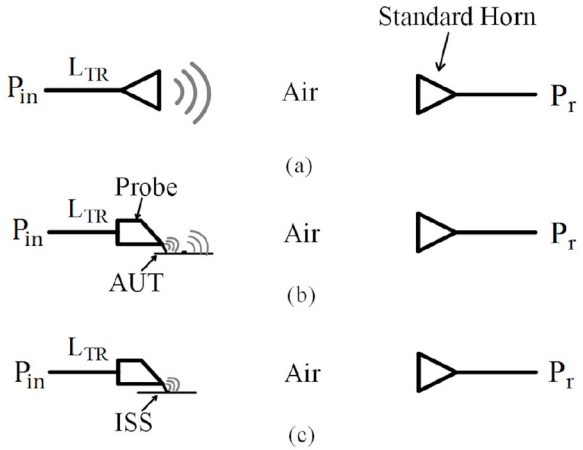

FIGURE 2. Illustration of the antenna radiation test principle.

an ACP40-GSG-100 is modelled, the probe structure and radiation mechanism are explained, and the simulated and measured probe radiation patterns and realized gain values are given. In Section IV, the effect on antenna radiation tests caused by probe radiation is analyzed with the help of a simple mathematical model. Finally, the conclusion is drawn in Section V.

II. ANTENNA MEASUREMENT SETUP AND TEST METHOD

A. PROBE-BASED MMWAVE ANTENNA MEASUREMENT SETUP

The probe-based mmWave antenna measurement setups have been developed over the last twenty years [31]. Our setup is a quasi-in-air-based far-field antenna measurement system settled in an anechoic chamber (size: 3.5m × 3.5m × 2.8m) with tapered absorbing material fully covering on its inner wall, as seen in Fig. 1. It undertakes the tasks to measure impedance, gain, and (3-D) radiation pattern of various types of antennas in different polarizations. Probe, waveguide, and coaxial-fed antennas are measurable at 60 cm spherical far-field condition from 18 GHz to 325 GHz currently.

The key equipment to realize scanning is the rotating stage that is a platform mainly comprises of two combined robotic arms with 0.1° positional accuracy. One of the arms is used for azimuth scanning (called φ-arm) and the other θ-arm is for 360° elevation scanning. The θ-arm carries a mmWave frequency converter with a standard receiving horn antenna connecting on it, the horn is always pointing at the AUT at far field distance during rotation.

More detailed information of the setup can be found in [31]. The coordinate system used in this paper is illustrated by the yellow arrows in Fig. 1. The origin of the coordinates is set on the probe tips (the coordinate system in the figure is moved to the floor for clear display), which is the position we commonly place the AUT. The angle from the positive z-axis is represented by θ, while φ represents the angle from the positive x-axis.

B. TEST METHOD ON AUT'S RADIATION

1) RADIATION PATTERN

To measure a radiation pattern, the AUT fed by the probe stays still on the AUT holder. The computer sends the movement trajectories to the rotating stage, the robotic arms rotate the receiving horn antenna around the AUT. The VNA is triggered to record the S_{21} parameter when the arms rotate to specified testing directions, the data is then post-processed and forms the radiation pattern.

2) REALIZED GAIN

The AUT's realized gain is implemented using the gain comparison method as illustrated in Fig. 2. P_{in} is the input power that comes out of the VNA, P_{out} is the output power that is obtained by the receiver. The S_{21} is the data that can be recorded by the setup directly. Fig. 2(a) is the case where the transmitting and receiving antennas are both standard horns whose gain is known in advance. The insertion loss between the transmitting and receiving interfaces (S_{21a}) can be measured.

Then, the transmitting horn is replaced by a probe feeding an AUT, as seen in Fig. 2(b). S_{21b} is then measured. Finally, we can calculate AUT's gain as:

$$G_{AUT} = S_{21b} - S_{21a} + L_{Probe} + G_{horn} \quad (1)$$

where L_{Probe} is a known parameter given by the probe manufacturer and G_{horn} is a known parameter given by the horn manufacturer.

Using (1) to obtain antenna gain can usually be accurate enough and has been widely accepted. However, a problem is that it ignores probe radiation. L_{Probe} is the insertion loss, which may not takes into account the fact that a part of it is actually dissipated in the form of radiation and received by the receiver, then mixes with AUT's radiation power. This unconscious system error will affect the testing accuracy

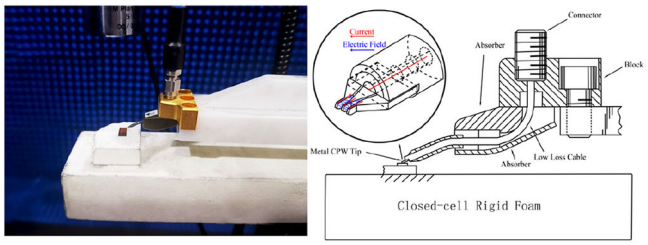

FIGURE 3. Photograph and schematic of ACP.

on antenna realized gain. It is necessary to know first why and how the probe radiates, how the probe radiation affects AUT's radiation, and thereby correct (1) to make it more accurate.

To study the pure radiation from the probe, referring to Fig. 2(c), we have:

$$G_{Probe} = S_{21c} - S_{21a} + L_{Probe} + d + G_{horn}. \quad (2)$$

Formula (2) considers the decomposition in probe's insertion loss, the correction factor d is the radiation loss content, and its value has to be simulated with a proper probe model. We chose ACP-40-GSG-100 as an example.

III. A CASE STUDY ON ACP-40-GSG-100

A. PROBE MODELING

Microelectronic probes with the GSG tips are widely used for feeding mmWave integrated antennas. The *Air Coplanar Probe* (ACP) developed by *Cascade Microtech, Inc.* adopts beryllium copper as air-isolated coplanar tip material, probe tips are designed to be at 23° to the horizontal plane and is suitable for rugged, repeatable contact on gold pads [10]. The signal transmission line consists of three parts: a coaxial connecter that links the external device to the probe, an air coplanar waveguide-based probe tips, and a coaxial line that connects the coaxial connector and the probe tips, see the ACP diagram in Fig. 3. The shell of the probe is mostly made of metal or hard absorbing material, yet the absorber cannot wrap the probe tip completely.

The probe tips are irregular structure made of metal cutting. ACP-40-GSG-100 has three probe tips with 100-μm tip pitch and operates up to 40 GHz. The signal tip in the middle is connected with the inner core of the coaxial line, the other two connect the ground of the coaxial line. Since the original model of the probe is not available, we used a microscope to observe the sizes of the probe tips. Then, a simulation model of the probe is built in HFSS software as shown in Fig. 4(a). Fig. 4(b) illustrates the model after adding probe's shell. The above two models are fed through the same interface. Fig. 4(c) gives the detailed size parameters of the probe tips.

The characteristics of the probe are verified in the simulation software. Fig. 5 shows the simulated reflection coefficient of the tips-isolated (open-ended) probe and the 50-Ω matched probe, both without shell. The S_{11} of the open-ended probe shows the total reflection characteristic

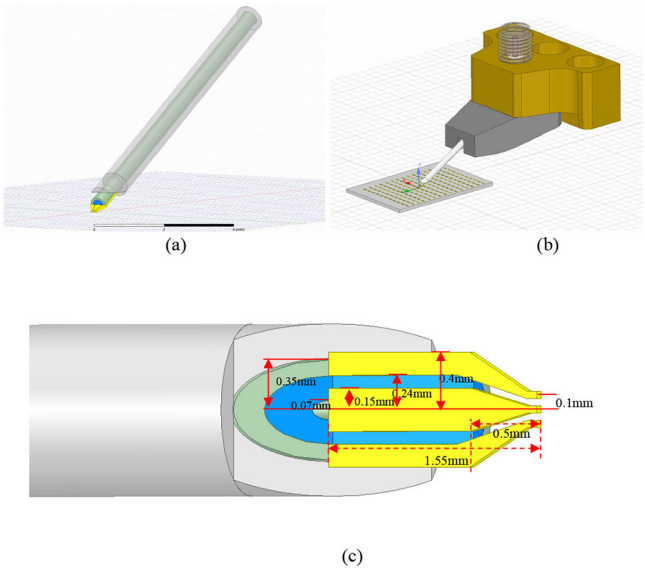

FIGURE 4. (a) Model of the ACP probe without the probe shell, (b) model of the ACP probe with the probe shell and an ISS, (c) Some size parameters of the probe.

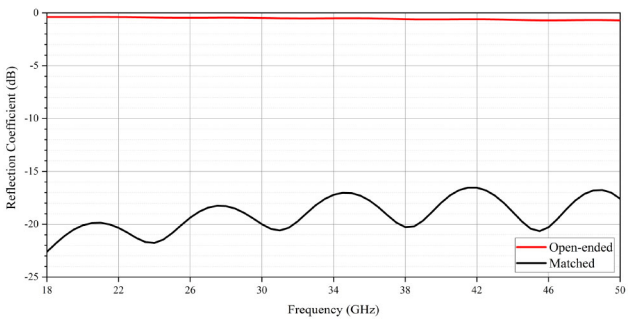

FIGURE 5. Simulated reflection coefficient of open-ended and matched ACP-40-GSG-100.

with its value more than −0.8 dB from 18 to 40 GHz, while the matched probe shows the matching characteristic with the value below −17 dB. These data are basically consistent with those obtained from the references. For example, at 28 GHz, the simulated insertion loss LProbe of the matched probe is 0.483 dB, the data in [11] is 0.49 dB; our simulated reflection coefficient is about −18.2 dB, and −23 dB data is given in [11]. However, the insertion loss from the datasheet given by the probe manufacturer is 0.057 dB, the difference is caused by the discrepancies in size parameters of our model and the actual probe.

B. RADIATION MECHANISM

The probe tips are symmetrical structure and can be regarded as an air CPW (ACPW). Power leakage of a conventional CPW has been calculated in [32], yet the result disagrees with our simulation on the ACPW tips. The dielectric medium has a strong effect on the electric field leakage in the conventional CPW, and thus the maximum leakage power radiates along the plane parallel to the ground. It is quite different in an ACPW, without the dielectric medium

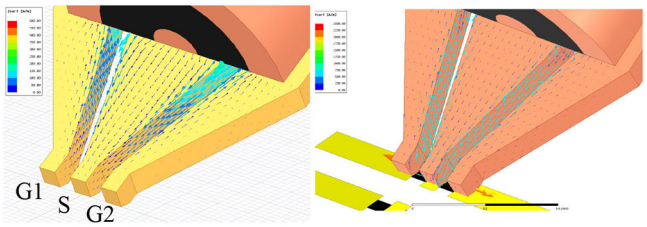

FIGURE 6. Simulated surface current on (a) open-ended, (b) matched probe tips.

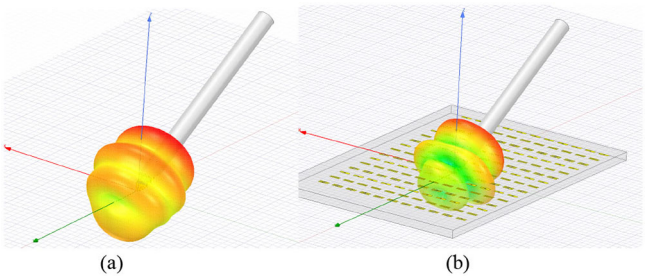

FIGURE 7. Simulated realized gain of the (a) open-ended, (b) matched probe without shell.

and ground plane, the metal surface current on the probe tips is symmetric about the yoz-plane and mainly distributed on the metal sidewall, as seen the simulated surface current of the probe tips in Fig. 6. The current mainly comes out from the S-tip and travels along its both sides, there are still some smaller currents distributed along the upper and lower surfaces. G1-tip has induced current on the side facing to the S-tip, with intensity equal but reverse in the travelling direction, so is the G2-tip. These currents are only 50 μm apart and behave like cancelling each other, but cannot completely offset, and thus will result in far-field radiation. Although the currents on the upper and lower surfaces of the S-tip have lower intensity, without the offsetting effect, these currents will excite radiation directly. By comparing the magnitude of the surface current on the differently terminated probes in Fig. 6, it is found that the current on the matched probe tip is indeed significantly larger in amplitude than the open-ended one, so the matched probe will certainly have stronger radiation or higher gain.

C. RADIATION CHARACTERISTICS

1) SIMULATION ON THE PROBE MODEL

To observe probe's intrinsic radiation, 3-D realized gain of the probe model (without shell) is simulated at 28 GHz. As seen from Fig. 7(a), the pattern shows a regular shape, and the maximum realized gain (−19.72 dBi) appears at the position where $\theta = -20°$, $\varphi = 90°$, a null appears at $\theta = 90°$. Fig. 7(b) shows the 3-D realized gain of the probe when terminating with a 50-Ω load printed on the ISS. It can be seen that the distribution of the probe radiation is basically the same as that of the open-ended probe, but the peak realized gain is 4.76 dB greater, reaches to −14.96 dBi.

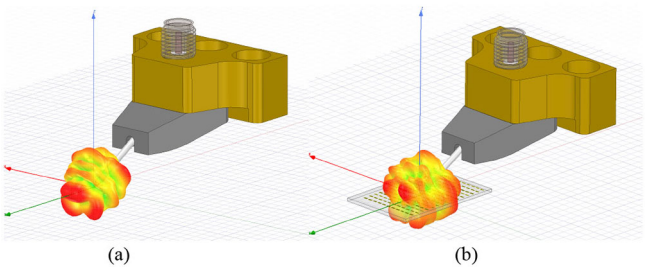

FIGURE 8. Simulated 3-D radiation patterns of the (a) open-ended probe, (b) matched probe with shell.

When studying the complete probe radiation with the reflection/scattering/diffraction from the probe shell, the metallic shell was added (shown in Fig. 8) for simulation.

Comparing the simulation results in Fig. 8 with those in Fig. 7, it is seen that the probe shell has strong effects on the radiation distribution and makes it quite unpredictable. Especially when the probe is matched on the ISS, more peaks and nulls appear. The peak realized gain of the open-ended probe with the shell turns to −18.2 dBi at $\theta = 94°$ and $\varphi = 79°$ (open-ended probe without shell: −19.72 dBi at $\theta = -20°$ and $\varphi = 90°$); the matched probe with the shell has −14.38 dBi peak realized gain at $\theta = 75°$ and $\varphi = 72°$ (matched probe without shell: −14.96 dBi at $\theta = -16°$ and $\varphi = 90°$), they basically locate at a plane where φ is close to 90°, i.e., between a narrow region near probe's yoz-plane.

The above simulations indicate the fact that the matched probe has higher realized gain than the open-ended one, which has verified what we inferred from the surface current distribution of the probe.

2) MEASUREMENT VALIDATION

Experimental verification on the probe radiation is then carried out in our setup. Part of the test equipment is shown in Fig. 9(a).

First, the test capability of the setup has to be assessed. A pair of identical standard horn antennas with gain of 11.64 dBi were used, the measured S_{21} level was −38.77 dB at 28 GHz. Then, we completely blocked the radiation from the transmitting horn antenna, the S_{21} level was measured from 18 GHz to 40 GHz, which is shown in Fig. 9(b). the S_{21} level was reduced to about −102.67 dB at 28 GHz.

We restored the prototype shown in Fig. 8 in the test environment. The xoz-plane and yoz-plane are chosen as the studied planes. The receiving horn antenna has excellent linear polarization characteristics. Therefore, by rotating the horn for 90°, the cross-polarized gain pattern can be measured.

3) RESULTS AND DISCUSSIONS

The simulated and measured gain patterns of the ACP40-GSG-100 probe are compared on the yoz-plane and xoz-plane for the θ-polarization ('simgaintheta' and 'meagaintheta') and the φ-polarization ('simgainphi' and 'meagainphi') at 28 GHz, as shown in Fig. 10(a). The total

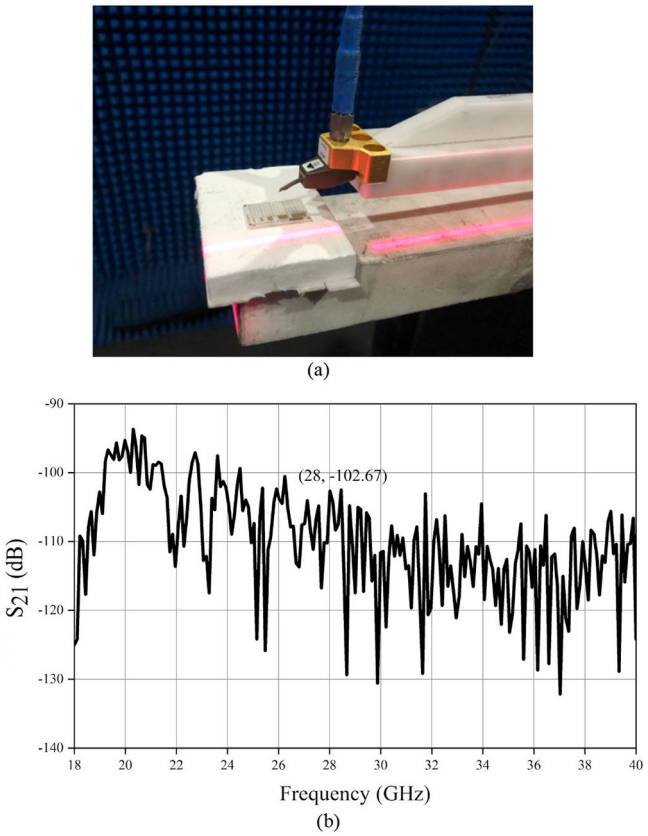

FIGURE 9. (a) Photograph of ACP40-GSG-100 and ISS, (b) measured S_{21} of the system from 18 to 40 GHz when the transmitting horn antenna was completed blocked.

realized gain is calculated using the dual polarization synthesis of 'gaintheta' and 'gainphi', as shown in Fig. 10(b). The parameter δ in (2) is not easy to obtain in experiment, so we acquired the value by simulating and post-processing the radiation efficiency of the probe, which is -0.043 dB at 28 GHz.

It is found that when the ACP is open-ended, the cross-polarized gain is 20 dB lower than the co-polarized gain at 28 GHz. Simulated and measured results both confirm this, which convinced us of the applicability of the model. However, the simulated and measured gain patterns have differences, which is caused by the differences between the probe and its model. Owing that the realized gain fits well, the difference is acceptable. It can be seen from the results that the matched probe indeed has higher realized gain than when it is open-ended, this agrees with our simulation.

We then scan the 3-D gain pattern of the matched ACP as shown in Fig. 11(a), we can find its -14.93 dBi peak realized gain locates at $\theta = 40°$ and $\varphi = 95°$ (simulation: -14.38 dBi, $\theta = 75°$ and $\varphi = 72°$), the discrepancy between the simulated and measured peak realized gain is about 0.55 dB. The measured peak gain locates at a plane where its φ is close to 90°, which is consistent with simulation. In simulation, the symmetry is exhibited when the probe is matched on an ISS as seen in Fig. 8(b), it becomes less asymmetrical in the tested result in Fig. 11(a). In order to

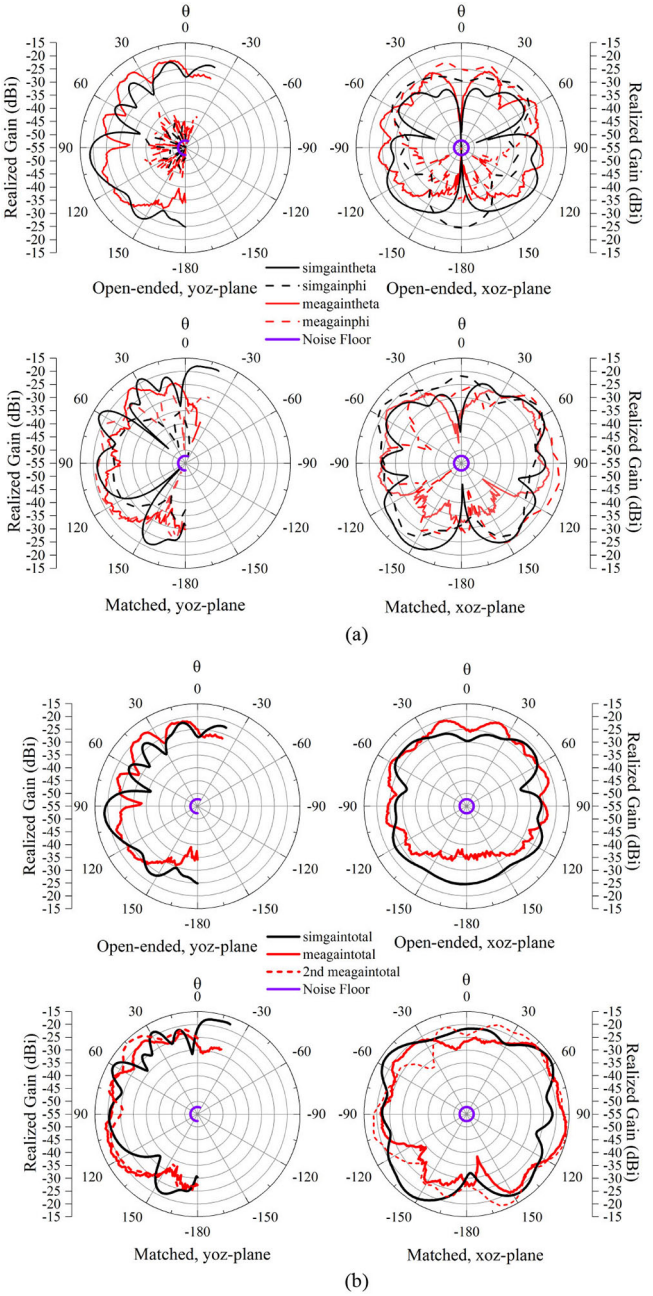

FIGURE 10. (a) Open-ended and matched ACP40-GSG-100's co-polarized and cross-polarized realized gain patterns at xoz-plane and yoz-plane at 28 GHz, (b) Open-ended and matched ACP40-GSG-100's total realized gain patterns.

further validate the symmetric feature, we performed another 3-D far-field scanning on an Infinity probe I75-T-GSG-150-BT at 60 GHz, as illustrated in Fig. 11(b). We find its peak realized gain locates at $\theta = 21°$ and $\varphi = 96°$, also near the $\varphi = 90°$ plane within a narrow region. Commonly, we regard probe's peak gain as the system sensitivity in antenna gain tests, and this knowledge instructs us to find the system sensitivity more rapidly. To be specific, we only need to scan a narrow beam according to the simulation result, this will save a lot of testing time.

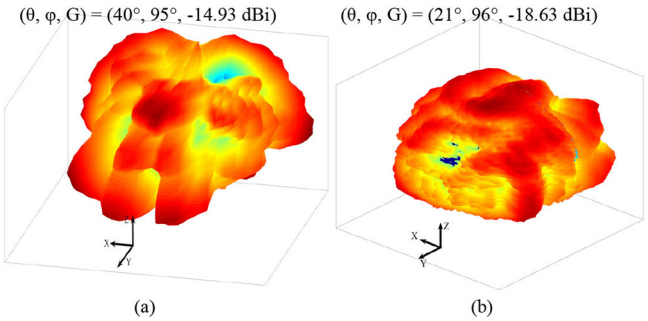

FIGURE 11. (a) Measured 3-D total realized gain pattern of ACP40-GSG-100 at 28 GHz, (b) Measured 3-D total realized gain pattern of Infinity I75-T-GSG-150-BT at 60 GHz.

Generally, measured results are often deviated from the simulated results. The reason is that at such tiny scale as the probe tips, measurement is often interfered by many factors. We have studied the impact when the probe tips contact on the different match loads printed on the ISS as an example. The red dash curve marked by '2nd meagain-total' in Fig. 10(b) is the radiation pattern after changing another match load on ISS. It is seen that the gain is basically the same, while radiated energy distribution has some differences. The patterns on the yoz-plane have the same fluctuating trend. The difference in the radiation pattern on the xoz-plane is quite severe. The discrepancies are mainly due to the difference between the reflection and coupling impacted by the gold feed pad. Another discovery is that if the probe tip is lifted and pressed again, or pressed at different depths, the radiation characteristics of the probe have almost no change. This guides us to try our best to feed the probe tips at the same feeding point during testing, so as to minimize the random errors caused by feeding differences.

Besides, we found that the realized gain of I75-T-GSG-150-BT is about 3.7 dB less than ACP40-GSG-100 and with a smoother radiation pattern, which indicates that different types of probes have different radiation characteristics, every probe require independent evaluation for its radiation characteristics.

D. TESTING RESULTS ON SOME TYPICAL PROBES

A few commonly used probes have been tested for their realized gain when matched on ISS to provide some possible reference, as seen in Table 1. Operating frequencies are chosen at those frequently used ones. ACP-40-GSG-100 has too little δ (−0.043 dB) to affect the test accuracy, which means the probe has an excellent performance, while some other probes are not as good as ACP-40-GSG-100. It is seen from Table 1, when probe's operating frequencies become high, absolute value of δ usually increases, which means this afore-ignored system error brings great challenges to measure at very high frequency, and it is necessary to be considered during calculations. Owing that lack of models, we only give the value interval of δ.

TABLE 1. Measured antenna gain of the probes.

Probe model	Frequency (GHz)	Realized gain (dBi)	δ (dB)
ACP65-GSG-150 (DC-65 GHz)	50	-11.80+δ	[-0.57, 0]
	65	-7.53+δ	[-0.80, 0]
I75-T-GSG-150-BT (50 - 75 GHz)	50	-17.99+δ	[-1.31, 0]
	60	-18.63+δ	[-0.91, 0]
	75	-14.72+δ	[-0.88, 0]
I110-T-GSG-150-BT (75 - 110 GHz)	79	-11.75+δ	[-1.29, 0]
	90	-15.07+δ	[-1.19, 0]
	110	-10.48+δ	[-1.64, 0]
Model 170-GSG-100-M (110 - 170 GHz)	122.5	-16.50+δ	[-2.08, 0]
	140	-14.40+δ	[-2.10, 0]
	160	-9.36+δ	[-2.10, 0]

Note: ACP and Infinity probes are produced by *Cascade Microtech. Inc.* Model series probe is produced by *GGB Industries, Inc.*

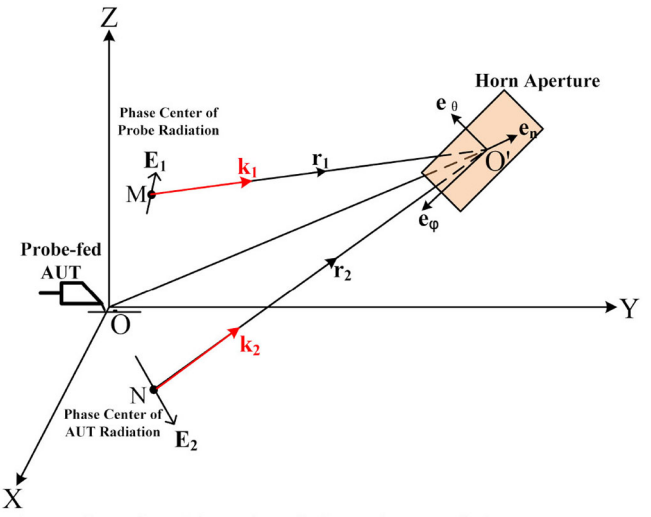

FIGURE 12. Illustration of the probe radiation and AUT radiation.

IV. ANALYSIS ON PROBE RADIATION EFFECTS

Having known about probe's self-radiation, it is also interested to know how the radiation affects the radiation measurements on AUTs. With the following analysis on the probe radiation's effects, it concludes that using low-gain probes will reduce the interference of probe radiation.

As seen the Fig. 12. The AUT is fed by a probe and they are put at the coordinate origin O, the receiving horn antenna is pointing to the origin and scans around it, i.e., $\mathbf{e_n} = \widehat{\mathbf{OO'}}$ ($\mathbf{e_n}$ is the unit normal vector of the horn aperture's center point O'). The probe radiation and the AUT have different phase center and usually are not locate at O point, and so we denote them as M point and N point respectively, their radiated electric field at a certain moment is $\mathbf{E_1}$ and $\mathbf{E_2}$. $\mathbf{k_1}$ and $\mathbf{k_2}$ are the propagation constants with directions of **MO'** ($\mathbf{r_1}$), **NO'** ($\mathbf{r_2}$) and they are equal in absolute value.

The receiving horn we utilized is a fine linear polarization antenna, which we concern only the Poynting vector ($\mathbf{S}$) composed of the electric field in the $\mathbf{e_\theta}$ direction and the orthogonal magnetic field in $\mathbf{e_\varphi}$ will be detected. The final detected electric fields are $\mathbf{E_1}$ and $\mathbf{E_2}$'s components on the θ direction when they transport to the horn aperture, which

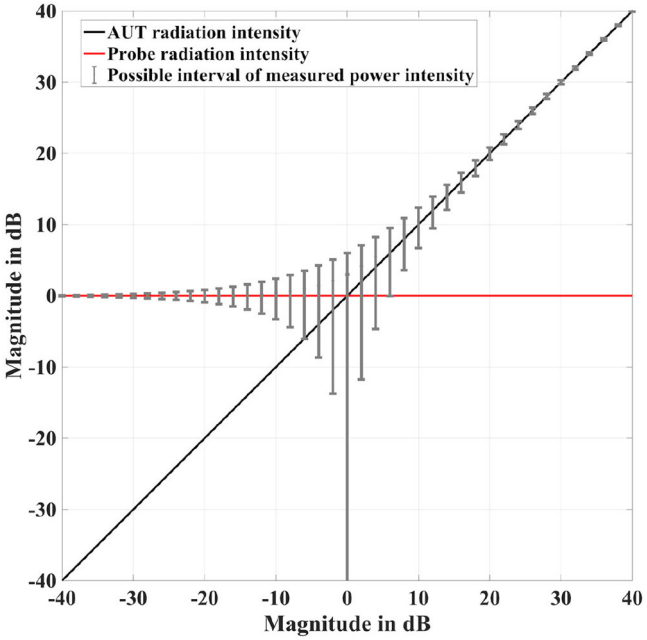

FIGURE 13. Calculation on the probe radiation's effect on antenna radiation tests.

is written as:

$$\mathbf{E_{1\theta}} = \mathbf{E_1} \cdot \mathbf{e_\theta} \cdot \mathbf{e}^{-\mathbf{i}\varphi_1} \cdot \mathbf{e_\theta} \tag{3}$$

$$\mathbf{E_{2\theta}} = \mathbf{E_2} \cdot \mathbf{e_\theta} \cdot \mathbf{e}^{-\mathbf{i}\varphi_2} \cdot \mathbf{e_\theta} \tag{4}$$

$$\mathbf{E} = \sum_i \mathbf{E_{i\theta}} \tag{5}$$

where $\varphi_\mathbf{i} = \mathbf{k_i} \cdot \mathbf{r_i} - \mathbf{\Phi_i} - \omega t$ represents the wave phase at the horn aperture, $\mathbf{\Phi_i}$ is the initial propagation phase of $\mathbf{E_i}$. $\mathbf{E}$ is the total detected electric field. The average value of the Poynting vector in a cycle time is:

$$<\mathbf{S}> = \frac{1}{2}\mathbf{e_n}\sqrt{\frac{\varepsilon}{\mu}}\mathrm{E}^2 \tag{6}$$

In our actual measurement, power intensity $\mathrm{I_i} = \mathrm{E_i^2}$ is enough to be used to characterize the relative captured EM power. The total received EM power is the synthesis of $\mathbf{E_{1\theta}}$ and $\mathbf{E_{2\theta}}$:

$$\mathrm{I} = \mathbf{E}^2 = |\mathbf{E_{1\theta}}|^2 + |\mathbf{E_{2\theta}}|^2 + 2|\mathbf{E_{1\theta}}||\mathbf{E_{2\theta}}|\cos(\varphi_1 - \varphi_2). \tag{7}$$

From (7) it is known that in order to calculate the total received power intensity, one just need to know $\mathrm{I_1}$, $\mathrm{I_2}$, and their phase difference. For an analysis as a general case, the phase difference is an unknown parameter and can be any value in [0°, 360°], AUT's radiation power is supposed higher than the probe's for D dB (D can be negative), the total received power intensity compared with AUT's radiation power can be calculated as:

$$\mathrm{I} - \mathrm{I_2}\ (\mathrm{dB}) = 10 \cdot \log_{10}\left[1 + 10^{-\frac{\mathrm{D}}{10}} + 2 \cdot 10^{-\frac{\mathrm{D}}{20}} \cdot \cos(\varphi_1 - \varphi_2)\right] \tag{8}$$

Fig. 13 visually shows the possible total power value obtained by (8), pointed out with grey error bars. The probe radiation power is set as a reference, as the red line shows. Black line represents the AUT's radiation intensity, and D is set from [−40 dB, 40 dB] for observation.

It is obvious that when AUT's power is significantly larger (or less) than probe's, the total received power will be very close to AUT's (probe's), ignoring the effect of phase difference. In other words, the stronger the AUT radiates than the probe, the more insignificant the impact comes from the probe radiation, this is the reason why probes with low gain are more competitive and suggested. If the probe radiates much stronger, AUT's radiation will likely be submerged in the probe radiation power, this phenomenon is often observed at the far side lobes with low gain in antenna tests. If the probe radiation is comparable with AUT's, the composite power becomes elusive and error increases, especially when the electric fields are equivalent reverse, a possible null can appear. In our tests, it is found that the antenna radiation result is accurate and smoother at the test direction where the AUT has high antenna gain, while the result at some directions with quite low AUT gain often becomes elusive.

V. CONCLUSION

Commercial microelectronic probes have self-radiation that has not been given systematic studies. Common probe-based method to measure antenna gain has a system error that has seldomly been noticed, which is due to probes' radiation.

In this paper, probe radiation characteristics are studied. We chose an ACP as the main study case. With simulation and experimental validation, it was found that matched probe has larger realized gain than when it is open-ended because of the stronger current on the probe tips. The probe radiation is not influenced by how deep it pushes on ISS, whereas different contact position on ISS or different contact loads changes its radiation distribution. Probes usually have symmetrical radiation patterns because of the symmetry in structure, the peak realized gain mostly locate near the direction that is close to the symmetry plane, this helps a lot in finding the system's antenna gain test sensitivity. A correction factor is introduced to reduce the system error hided in the test method. With the correction, the gain data becomes more convincible.

The effects on antenna radiation tests caused by probe radiation are finally analyzed. Through this analysis, we confirmed how the probe radiation influences the AUT's gain, and why it is suggested to use probes with low realized gain as much as possible.

ACKNOWLEDGMENT

The authors would like to acknowledge Dr. Bin Xia for his support on the probe model and Jun Shu for his assistance on measurements.

REFERENCES

[1] M. K. Samimi and T. S. Rappaport, "3-D millimeter-wave statistical channel model for 5G wireless system design," *IEEE Trans. Microw. Theory Techn.*, vol. 64, no. 7, pp. 2207–2225, Jul. 2016.

[2] M. Alibakhshikenari, B. S. Virdee, C. H. See, R. A. Abd-Alhameed, F. Falcone, and E. Limiti, "High-isolation leaky-wave array antenna based on CRLH-metamaterial implemented on SIW with ±30° frequency beam-scanning capability at millimetre-waves," *Electronics*, vol. 8, no. 6, p. 642, 2019.
[3] M. Alibakhshikenari, B. S. Virdee, A. Ali, and E. Limiti, "Extended aperture miniature antenna based on CRLH metamaterials for wireless communication systems operating over UHF to C-band," *Radio Sci.*, vol. 53, no. 2, pp. 154–165, Feb. 2018.
[4] M. Alibakhshikenari *et al.*, "A comprehensive survey of 'metamaterial transmission-line based antennas: Design, challenges, and applications,"' *IEEE Access*, vol. 8, pp. 144778–144808, 2020.
[5] M. Alibakhshikenari *et al.*, "A comprehensive survey on 'various decoupling mechanisms with focus on metamaterial and metasurface principles applicable to SAR and MIMO antenna systems,"' *IEEE Access*, vol. 8, pp. 192965–193004, 2020.
[6] M. Alibakhshikenari, B. S. Virdee, C. H. See, R. A. Abd-Alhameed, F. Falcone, and E. Limiti, "High-gain metasurface in polyimide on-chip antenna based on CRLH-TL for sub-terahertz integrated circuits," *Sci. Rep.*, vol. 10, p. 4298, Mar. 2020, doi: 10.1038/s41598-020-61099-8.
[7] N. O. Parchin *et al.*, "Mobile-phone antenna array with diamond-ring slot elements for 5G massive MIMO system," *Electron.*, vol. 9, no. 5, pp. 1–14, 2019.
[8] Y. P. Zhang, M. Sun, K. M. Chua, L. L. Wai, and D. Liu, "Antenna-in-package design for wirebond interconnection to highly integrated 60-GHz radios," *IEEE Trans. Antennas Propag.*, vol. 57, no. 10, pp. 2842–2852, Oct. 2009.
[9] Y. P. Zhang and J. F. Mao, "An overview of the development of antenna-in-package technology for highly integrated wireless devices," *Proc. IEEE*, vol. 107, no. 11, pp. 2265–2280, Nov. 2019.
[10] E. M. Godshalk, J. A. Williams, and J. N. Burr, "High-frequency probe tip assembly," U.S. Patent 5 506 515, Apr. 9, 1996.
[11] E. M. Godshalk, J. Burr, and J. Williams, "An air coplanar wafer probe," in *43rd ARFTG Conf. Dig.*, San Diego, CA, USA, 1994, pp. 1380–1385.
[12] S. K. Rockwell and B. A. Bosco, "On-wafer characterization de-embedding and transmission line optimization on silicon for millimeter-wave applications," in *RFIC Symp. Dig.*, Jun. 2005, pp. 561–564.
[13] B. Rejaei, A. Akhnoukh, M. Spirito, and L. Hayden, "Effect of a local ground and probe radiation on the microwave characterization of integrated inductors," *IEEE Trans. Microw. Theory Techn.*, vol. 55, no. 10, pp. 2240–2247, Oct. 2007.
[14] L. Boehm, A. Foerstner, M. Hitzler, and C. Waldschmidt, "Reflection reduction through modal filtering for integrated antenna measurements above 100 GHz," *IEEE Trans. Antennas Propag.*, vol. 65, no. 7, pp. 3712–3720, Jul. 2017.
[15] K. V. Caekenberghe *et al.*, "A 2–40 GHz probe station based setup for on-wafer antenna measurements," *IEEE Trans. Antennas Propag.*, vol. 56, no. 10, pp. 3241–3247, Oct. 2008.
[16] R. N. Simons and R. Q. Lee, "On-wafer characterization of millimeter-wave antennas for wireless applications," *IEEE Trans. Microw. Theory Tech.*, vol. 47, no. 1, pp. 92–96, Jan. 1999.
[17] T. Zwick, C. Baks, U. R. Pfeiffer, D. Liu, and B. P. Gaucher, "Probe based MMW antenna measurement setup," in *Proc. IEEE AP-S Int. Symp.*, vol. 1, Jun. 2004, pp. 747–750.
[18] S. Beer, G. Adamiuk, and T. Zwick, "Design and probe based measurement of 77 GHz antennas for antenna in package applications," in *Proc. Eur. Microw. Conf.*, Sep. 2009, pp. 524–527.
[19] S. Beer and T. Zwick, "Probe based radiation pattern measurements for highly integrated millimeter-wave antennas," in *Proc. Eur. Conf. Antennas Propag.*, Apr. 2010, pp. 1–5.
[20] H. Gulan *et al.*, "Probe based antenna measurements up to 325 GHz for upcoming millimeter-wave applications," in *Proc. IEEE Int. Workshop Antenna Technol.*, Karlsruhe, Germany, Mar. 2013, pp. 228–231.
[21] S. Ranvier, M. Kyrö, C. Luxey, R. Staraj, C. Icheln, and P. Vainikainen, "Compact 3-D on-wafer radiation pattern measurement system for 60 GHz antennas," *Microw. Opt. Tech. Lett.*, vol. 51, no. 2, pp. 319–324, Feb. 2009.
[22] D. Titz, M. Kyrö, C. Luxey, F. Ben Abdeljelil, G. Jacquemod, and P. Vainikainen, "Radiation pattern measurement set-up for 60 GHz on-chip antennas," in *Proc. Loughborough Antennas Propag. Conf. (LAPC)*, 2010, pp. 533–536.
[23] D. Titz, F. Ferrero, C. Luxey, and G. Jacquemod, "A novel fully-automatic 3D radiation pattern measurement setup for 60 GHz probe-fed antennas," *Proc. IEEE Int. Symp. on Antennas Propag. (APSURSI)*, Spokane, WA, USA, Jul. 2011, pp. 3121–3124.
[24] D. Titz, F. Ferrero, and C. Luxey, "Development of a millimeter-wave measurement setup and dedicated techniques to characterize the matching and radiation performance of probe-fed antennas [measurements corner]," *IEEE Antennas Propag. Mag.*, vol. 54, no. 4, pp. 188–203, Aug. 2012.
[25] B. E. Fischer, I. J. LaHaie, M. D. Huang, M. H. A. J. Herben, A. C. F. Reniers, and P. F. M. Smulders, "Causes of discrepancies between measurements and em simulations of millimeter-wave antennas [measurements corner]," *IEEE Antennas Propag. Mag.*, vol. 55, no. 6, pp. 139–149, Dec. 2013.
[26] L. Boehm, F. Boegelsack, M. Hitzler, and C. Waldschmidt, "An automated millimeter-wave antenna measurement setup using a robotic arm," in *Proc. Int. Symp. IEEE Antennas Propag. USNC/URSI Nat. Radio Sci. Meet.*, Vancouver, BC, Canada, 2015, pp. 2109–2110.
[27] L. Boehm, F. Boegelsack, M. Hitzler, and C. Waldschmidt, "The challenges of measuring integrated antennas at millimeter-wave frequencies [measurements corner]," *IEEE Antennas Propag. Mag.*, vol. 59, no. 4, pp. 84–92, Aug. 2017.
[28] M. Seyyed-Esfahlan, M. Kaynak, B. Göttel, and I. Tekin, "SiGe process integrated on-chip dipole antenna on finite-size ground plane," *IEEE Antennas Wireless Propag. Lett.*, vol. 12, pp. 1260–1263, 2013.
[29] L. Marnat, A. A. A. Carreno, D. Conchouso, M. G. Martínez, I. G. Foulds, and A. Shamim, "New movable plate for efficient millimeter wave vertical on-chip antenna," *IEEE Trans. Antennas Propag.*, vol. 61, no. 4, pp. 1608–1615, Apr. 2013.
[30] Z. Zheng and Y. P. Zhang, "A study of a probe-based millimeter-wave far-field antenna measurement setup [measurements corner]," *IEEE Antennas Propag. Mag.*, vol. 63, no. 5, pp. 118–144, Oct. 2021.
[31] Z. Zheng, Y. Zhang, L. Shi, L. Wu, and J.-F. Mao, "An overview of probe-based millimeter-wave/terahertz far-field antenna measurement setups [measurements corner]," *IEEE Antennas Propag. Mag.*, vol. 63, no. 2, pp. 63–118, Apr. 2021.
[32] C.-F. Hung, A.-S. Liu, C.-H. Chien, C.-L. Wang, and R.-B. Wu, "Bandwidth enhancement on waveguide transition to conductor backed CPW with high dielectric constant substrate," *IEEE Microw. Wireless Compon. Lett.*, vol. 15, no. 2, pp. 128–130, Feb. 2005.